2019-01-0950

# Effects of Single versus Two-Stage Heat Release on the Load Limits of HCCI using Primary Reference Fuels

**Author, co-author (Do NOT enter this information. It will be pulled from participant tab in MyTechZone)**

Affiliation (Do NOT enter this information. It will be pulled from participant tab in MyTechZone)

## Abstract

Homogeneous Charge Compression Ignition (HCCI) enables combustion with high efficiency and low emissions. Control over the combustion process and its narrow operating range are still the biggest challenges associated with HCCI. To expand the operable load ranges of HCCI, this paper explores the effects of single versus two-stage ignition fuels by studying the Primary Reference Fuels (PRF) in a variable compression ratio Cooperative Fuel Research (CFR) engine. The PRF fuels, iso-octane and n-heptane, are blended together at various concentrations to create fuel blends with different autoignition characteristics. Experiments were conducted using these PRF blends to explore the extent to which the load range can be extended with two-stage ignition fuels at various compression ratios and intake temperatures. The reactivity of the PRF blends increases with the fraction of n-heptane and so does the amount of low temperature heat release (LTHR).

Since the low PRF number fuels have a higher reactivity, they can be autoignited at very low compression ratios while maintaining comparable combustion phasing and equivalence ratios. At the lower compression ratios, the low load limits were found to be extended while maintaining high combustion efficiencies. Additionally, lower peak pressures and pressure rise rates were achieved at low PRF number fuels as a result of its two-stage heat release, which can be used to reach higher loads. In addition, the energy released from the LTHR can be used to delay the CA50 combustion phasing (i.e., the crank angle timing where 50% of the energy has been released) beyond what is possible with a single-stage ignition fuel, which allows further high load extension. However, using lower compression ratios has a negative impact on the thermal efficiency. The effects of the extended load, single- and two-stage heat release, combustion phasing, and equivalence ratios on combustion efficiency, thermal efficiencies, and combustion durations were also explored.

## Introduction

Homogeneous Charge Compression Ignition (HCCI) is a Low Temperature Combustion (LTC) mode in which a lean, homogeneous mixture of fuel and air is autoignited to produce thermodynamic work. Lean operation provides efficiencies as high as conventional Compression Ignition (CI) engines while low-temperature, homogeneous operation provides emissions as low as Spark Ignition (SI) engines with aftertreatment. However, HCCI lacks a means of controlling the heat release process, resulting in a narrow operating load range that prevents HCCI operation in a commercial setting. In HCCI, there is neither a spark plug nor a direct fuel injector to control the start of combustion (SOC) or rate of combustion. Instead, the SOC and rate of combustion depends mainly on chemical kinetics and the maximum temperature [1 – 6], and the natural in-cylinder thermal stratification [7 – 12], respectively. Due to the lack of direct control over the SOC and the burn rate, the operating load range of HCCI is limited to the low-to-mid load range of conventional combustion modes [13]. Engine load is the volume-normalized thermodynamic work output from combustion, irrespective of the engine size, combustion mode, and combustion characteristics, expressed as a Mean Effective Pressure (MEP).

The low- and high-load limit of the HCCI operating range are defined by different factors. At low loads, the fuel-air mixture is excessively lean, lowering peak combustion temperatures and making autoignition more difficult. This results in incomplete combustion, i.e., higher total unburned hydrocarbons (THC) and CO emissions, and misfire. Contrarily, at high loads, the fuel-air mixture becomes richer and the energy release rates become excessively high. This results in high pressure rise rates, which contribute to the audible noise of the engine and can physically damage the combustion chamber and piston.

Saxena et al. [14] discussed various limitations that prevent high load operation in HCCI and LTC, along with the strategies that researchers have used to overcome these limitations. The high load limit of LTC is often defined by a Maximum Pressure Rise Rate (MPRR) limit. Two proposed methods to lower the MPRR at high loads are delaying the combustion phasing and elongating the heat process. Elongating the heat release can be done by taking advantage of thermal stratification [15 – 18] and/or an intentional equivalence ratio stratification. Researchers have studied different methods to induce thermal stratification by the injection of either water [19 – 21] or wet ethanol [22, 23]. The latent heat of vaporization of the directly injected fuel/water caused an increase in the thermal stratification in the cylinder which reduces the peak heat release and pressure rise rates.

Delaying the combustion phasing is an effective way to extend the high-load limit. In general, this is done by retarding the start of combustion. Irrespective of engine speed, equivalence ratio, fuel, intake pressure, and engine load, the temperature of the intake air was found to be the most effective method to control the start of combustion in HCCI [24 – 26]. Decreasing the intake temperature causes the combustion phasing to retard. As the

piston moves away from Top Dead Center (TDC), the expansion rate increases [14]. The decrease in pressure due to expansion counteracts the increase in pressure due to combustion, elongating the burn duration. Therefore, later combustion phasing results in a lower MPRR.

Although delaying combustion phasing can extend the high-load limit of HCCI, it is detrimental to thermal efficiency [27]. Additionally, as combustion is phased later in the cycle, it can result in higher THC emissions. Late combustion phasing also results in higher exhaust losses, since the total available expansion work decreases [27]. Although the intake temperature was shown to be one of the most effective methods of controlling the combustion phasing, it has its own limitations. The intake temperature is generally inversely related to the engine load. Therefore, at very high loads, the required intake temperature becomes lower than the ambient temperature [14]. Under such conditions, the maximum obtainable load is limited by the intake temperature. Additionally, even though an intake heater is used most commonly in research to study the fundamental influence of different intake temperatures on combustion, it is unrealistic to use an intake heater in a production engine. The current strategies that are applicable to production engines are 1) using a heat exchanger with the hot exhaust gases to heat the intake charge entering the engine, 2) using variable valve timing with negative valve overlap (NVO) to control the amount of hot internal residuals that are trapped and retained from one cycle to the next, and 3) injecting fuel during the NVO period which partially reforms the fuel and produces more reactive species that have been shown to control combustion phasing.

Partial Fuel Stratification (PFS) is another method of controlling the heat release process in HCCI [26, 28 – 35]. This method is very effective for fuels that have a high equivalence ratio sensitivity [26, 33]. In PFS, a fraction of the total fuel is direct injected during the compression stroke to introduce an equivalence ratio stratification. Combustion will then occur sequentially starting from the richest regions and progressing to the leaner regions, which extends the burn duration. Extending the burn duration decreases peak pressure rise rates and heat release rates, and extends the high-load limit of LTC.

PFS has two limitations. First, the maximum fraction of fuel injected during the compression stroke has to be limited in order to mitigate locally rich regions that could result in higher NOx emissions or poor combustion efficiency [34]. Second, if the direct injection occurs too late in the compression stroke, there is not enough time for spray break-up and mixing, resulting in a fast-premixed combustion event followed by a diffusion combustion event. The premixed combustion event will result in high pressure rise rates while the diffusion combustion event will result in particulate emissions. Additionally, PFS is only effective for fuels with equivalence ratio sensitivity; fuels that do not exhibit a strong equivalence ratio sensitivity cannot be used [34, 35].

In addition to conventional fuels, the equivalence ratio sensitivities of the Primary Reference Fuels (PRF) have also been studied in the past [35 – 39]. Iso-octane and n-heptane are the two PRF fuels, which are blended together to produce different PRF blends. Due to pre-ignition chemistry, n-heptane undergoes a two-stage heat release process, similar to heavy hydrocarbons like diesel [37, 38, 40]. This two-stage heat release process includes a low temperature heat release (LTHR) event followed by a high temperature heat release (HTHR) event. Fuels that undergo pre-ignition chemistry to produce LTHR have shown a higher equivalence ratio sensitivity when compared to single-stage ignition fuels such as ethanol [36]. The LTHR occurs at temperatures between 750 K and 850 K [41 – 43], and fuels with paraffins usually produce LTHR more readily than non-paraffinic fuels [44]. Various researchers have studied the chemical kinetics and reaction pathways behind the LTHR and their influence on the LTHR and HTHR in detail [14, 45, 46].

Yang [35] studied the equivalence ratio sensitivity of the PRF fuels by comparing PRF73 (73% iso-octane and 27% n-heptane) and PRF100 (iso-octane). They found that CA10 of PRF73 advanced with an increase in equivalence ratio due to pre-ignition chemistry, while the CA10 of iso-octane retarded with an increase in equivalence ratio.

The LTHR presents the opportunity to both spread out the heat release event and potentially retard the combustion phasing beyond what is possible with a single-stage ignition fuel. Both the broader heat release process and the retarded combustion phasing could be used to extend the high load limit of HCCI. In this paper, the LTHR of primary reference fuels of different blends were studied on a single cylinder Cooperative Fuel Research (CFR) engine in HCCI combustion mode with the goal of exploring the high-load limit. The effects of equivalence ratio, compression ratio, intake temperature, and PRF blends on both the LTHR and HTHR were studied.

## Motivation

To explore the method of increasing the high-load limit of HCCI combustion by utilizing LTHR, the heat release characteristics of various PRF fuels are first analyzed. Figure 1 shows the gross heat release rate (GHRR) of four different PRF blends at various intake temperatures. In order to have a valid comparison between the heat release rates of different PRF blends with the same equivalence ratio, the combustion phasing was kept constant by adjusting the intake temperature. As the reactivity of the fuel increased (decreasing PRF number), the intake temperature requirement decreased to maintain a constant CA50 of 5 deg aTDC. All four of the cases in Figure 1 were conducted with a constant compression ratio of 9. Because of the higher intake temperature requirement for higher PRF blends, the mass of air inducted into the cylinder decreased slightly due to a decrease in air density. To compensate for the decrease in the mass of air, the mass of fuel was decreased so that the equivalence ratio remained constant, which explains the slight change in load between the four cases.

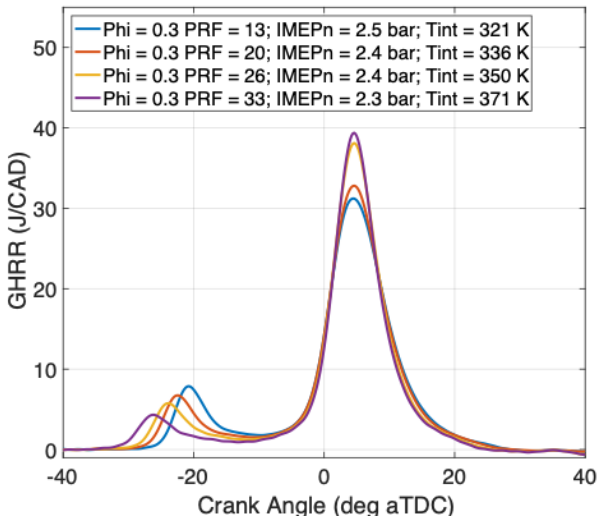


Figure 1: Gross heat release rate (GHRR) for varying PRF number and intake temperature at a constant combustion phasing and equivalence ratio

By examining the LTHR of the four cases in Figure 1, it becomes clear that the percentage of LTHR in the overall heat release is related to the PRF number. In fact, the fraction of the total heat release that is LTHR decreases from 12.8% to 8.9% as the PRF number of the fuel blend increases. This change was due to the decrease in the amount of n-heptane in the higher PRF fuels, since n-heptane is responsible for the LTHR produced by the fuel blend at these conditions. Beyond the changes to the fraction of the LTHR from the change to the percent of n-heptane, the start of the LTHR also changed for each case, even though the phasing of the HTHR was constant. Since both the PRF number and the intake temperature changed simultaneously, the reason that the start of LTHR changed could be either of those two parameters. In order to isolate their effects on the start of LTHR, experiments were conducted with a constant intake temperature but varying PRF number and compression ratio. As the PRF blends changed, the compression ratios also changed to maintain the combustion phasing constant. The GHRRs of different PRF blends at a constant intake temperature and equivalence ratio are shown in Figure 2.

Unlike the previous dataset, the start of LTHR in Figure 2 is approximately constant when the intake air temperature was kept constant at 350 K, and the equivalence ratio was kept constant at 0.3, irrespective of the PRF blend. Along with the start of LTHR, since the intake temperature was constant, the mass flow rate of air and fuel were also constant. The slightly higher load at PRF60 (2.5 bar versus 2.4 bar for the other cases) is attributed to the higher thermal efficiency at a compression ratio of 11, which will be discussed in more detail later. Additionally, the fraction of LTHR in the overall heat release decreased from 10% to 2% with the increase in PRF number, for the same reason as described earlier: due to the decrease of n-heptane in the fuel blends.

From Figure 1 and 2, it can be seen that the amount of LTHR is determined mainly by the PRF blend, and moderately by the temperature at the start of LTHR. However, the start of LTHR completely depends on the intake temperature and not the PRF blends. Since the start of LTHR changes with temperature, the amount of LTHR also changes, where a higher temperature and earlier LTHR phasing result in a lower peak of the LTHR. It also shows that, with a lower PRF number, a larger fraction of the total heat release will occur as LTHR. This results in a lower peak of the HTHR, which can be seen in both Figure 1 and Figure 2. These results illustrate that the fraction of LTHR could potentially be used to reduce the peak pressure rise rate and enable higher loads. Additionally, since the energy release from the LTHR helps initiate the HTHR, the combustion phasing of two-stage ignition fuels can be retarded beyond the range of single-stage ignition fuels. With later combustion phasings, it might be possible to extend the maximum load further. This paper attempts to first determine the factors that affect the fraction of LTHR specifically, and then determine the load limits and combustion phasing limits of single versus two-stage ignition fuels.

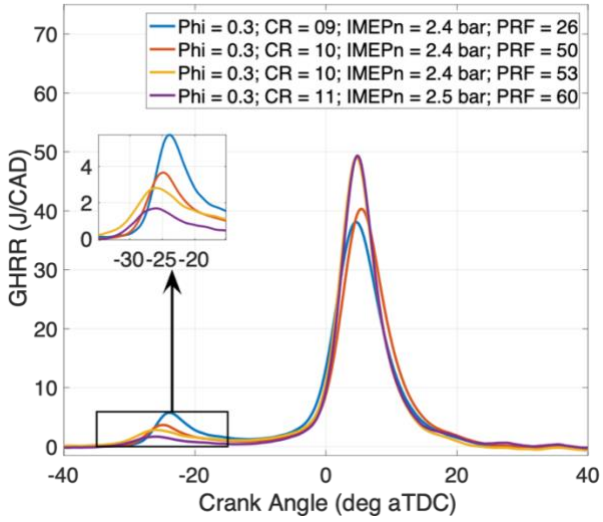


Figure 2: Gross heat release rate (GHRR) for various PRF blends at a constant intake temperature and equivalence ratio

## Methodology

### *Experimental setup*

Experiments were conducted on a single cylinder, spark ignition (SI), Cooperative Fuel Research (CFR) engine with a side-mounted spark plug at Stony Brook University's Advanced Combustion Research Laboratory. In this study, the engine was operated in HCCI combustion mode. The CFR engine is capable of varying its compression ratio, which is utilized in this paper to autoignite different PRF blends. Since controlling the intake temperature is an effective way to control the combustion phasing in HCCI, an inline intake heater was used to control the temperature of the intake air. The engine geometry and valve timings are listed in Table 1; Figure 3 displays a schematic view of the experimental test cell.

Table 1: Engine parameters

| | |
|---|---|
| Bore | 82.6 mm |
| Stroke | 114.3 mm |
| Connecting rod length | 254 mm |
| Compression ratio | 6:1 to 18:1 |
| Optical shaft encoder's resolutions | 0.2 Crank Angle Degrees (CAD) |
| Intake Valve Opening (IVO) | 12° deg aTDC |
| Intake Valve Closing (IVC) | -153° deg aTDC |
| Exhaust Valve Opening (EVO) | 141° deg aTDC |
| Exhaust Valve Closing (EVC) | 5° deg aTDC |

An Alicat mass flow controller was used to measure and control the intake mass flow rate of air. The liquid fuel was injected into the intake manifold with a PFI injector. The engine is also capable of operating on gaseous fuels which would be connected directly into the intake plenum through a mass flow controller. However, this was not used in this particular study. The mass flow rate of the fuel was measured using a Micro Motion Coriolis fuel flow meter. The air-fuel ratio of the experiments was measured using two methods to ensure accuracy. First, the air-fuel ratio was calculated based on the measured mass flow rates of fuel and air. Second, the air-fuel ratio was calculated based on the species composition of the emissions measured using a Horiba Mexa-7100 D-EGR motor exhaust gas analyzer. CO, $CO_2$, $O_2$, $NO_x$, $CH_4$ and total unburned hydrocarbons (THC) are measured directly using the analyzer and the measured values are used to calculate the air-fuel ratio using the Brettschnieder air-fuel ratio equation [47].

The in-cylinder pressure was measured using a water-cooled Kistler piezoelectric pressure transducer with a resolution of 0.2 CAD with the help of an encoder coupled to the engine's crankshaft. Omega PID controllers were used to control the coolant and oil temperatures, whereas a custom LabVIEW code was used to control and monitor all other pressures, temperatures, and flow rates. The engine flywheel is directly coupled to a 30 hp GE active DC dynamometer to maintain the engine speed at 1200 rpm throughout the experiments.

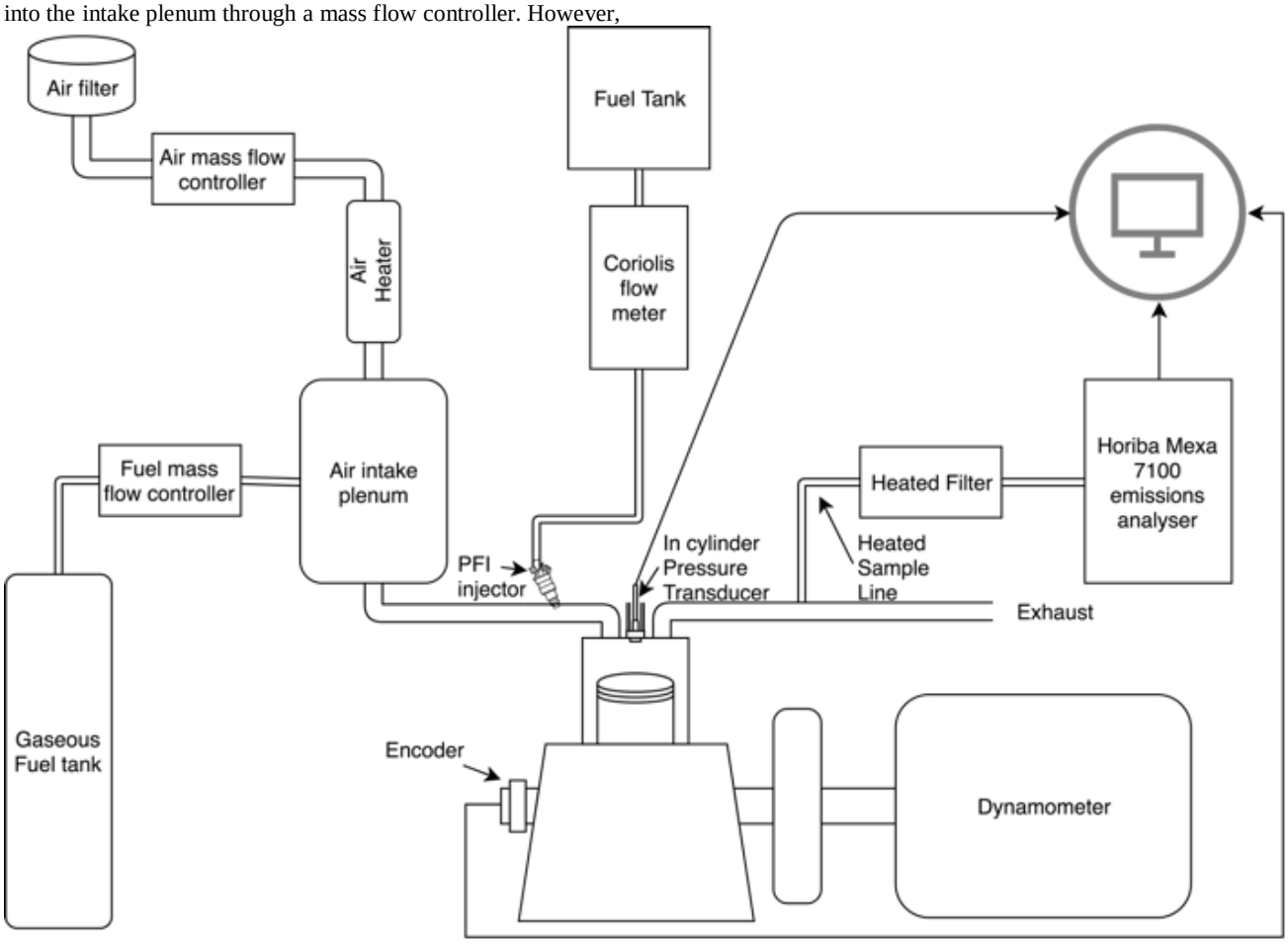


Figure 3: Schematic of the CFR engine test cell

The in-cylinder pressure was recorded for 200 consecutive cycles and their ensemble average has been filtered using a Butterworth filter with a cut-off frequency of ~5 kHz. The ensemble-averaged and filtered pressure trace was used to calculate the heat release rate and the bulk temperature for the closed portion of the cycle from IVC to EVO. Heat transfer losses were calculated for the same interval using the Modified Woschni heat transfer correlation [48]. The internal residual gas fraction was determined by using the measured intake and exhaust temperatures and the measured mass flow rates of fuel and air into the engine. The filtered pressure trace was also used to calculate the maximum pressure rise rate (MPRR), which is limited to less than 5 bar/CAD.

The effect of the intake temperature on various PRF fuel blends was studied at a constant combustion phasing and equivalence ratio above. The behavior of the LTHR was analyzed along with the fraction of the total heat release that occurs during the LTHR. Following that, the effect of intake temperature and PRF number were studied individually to investigate their effect on LTHR and HTHR at a constant combustion phasing and compression ratio under naturally aspirated intake conditions. Next, the maximum possible load was determined for PRF100, PRF50, and PRF0. Finally, with PRF0, the compression ratio was varied between 8 and 6.5, at a constant intake temperature of 350 K to understand the effect of the pressure at the start of combustion on the heat release rates. The intake temperature was fixed while the equivalence ratio was adjusted to achieve the desired combustion phasing at different compression ratios.

### *Modeling setup*

In order to better understand the experimentally observed trends of the heat release rate process, a single-zone, constant volume chemical kinetics model was used. The model was constructed in MATLAB using Cantera to solve the chemical kinetics [49]. The model uses a reduced mechanism with 73 species and 296 reactions by Wang [50]. The chemical kinetics simulations can capture how the LTHR changes with various operating conditions, including temperature, pressure, PRF number, and equivalence ratio. Additionally, the single-zone, chemical kinetic simulation can help isolate the effects of an individual parameter on the heat release rate, unlike the experiment where multiple parameters are coupled. The model was used to study the qualitative effect of the pressure (to simulate different compression ratios), equivalence ratio, and intake temperature on the LTHR of PRF0. The pressure and temperature at the start of combustion and the equivalence ratio are the three factors that were varied for this simulation study. Along with the heat release characteristics of individual cases, the fraction of LTHR was also simulated for a wide range of equivalence ratios and start of combustion pressures. In all cases, the heat release rates from the simulations were normalized by the total energy input to remove any differences in the total energy input due to differences in the density or equivalence ratio.

## Results and Discussion

First, the operable load limits of HCCI were determined for iso-octane (PRF100) with a compression ratio of 15. Figure 4 shows their gross heat release rates (GHRR). At the lowest loads, the intake temperature is the highest and the equivalence ratio is the lowest. To increase the load, the mass of fuel was increased gradually, while the intake temperature was decreases to maintain CA50 at 5 ± 0.5 deg aTDC. As the load increased at constant combustion phasing, the MPRR also increased. At an $IMEP_n$ of 3 bar, the MPRR reaches the limit of 5 bar/CAD, and can be seen in Table 2. Next, the intake temperature was reduced further to retard the combustion phasing. However, at a CA50 of 6 deg aTDC, the engine reached its stability/misfire limit. Later CA50 phasings caused the COV of IMEP to increase above 3%. The thermal efficiency was maximum for Case 3 (Table 2) at 42.3%, even though the IMEPn is highest for Case 4. This is due to the lower MPRR in Case 3, which results in less heat transfer losses. This result shows that the latest possible CA50 for iso-octane is 6 deg aTDC, the maximum $IMEP_n$ is 3 bar on this particular engine and at these conditions. If CA50 could have been retarded beyond 6 deg aTDC, higher loads would have been possible with an acceptable MPRR. Alternatively, a more pronounced LTHR event would reduce the peak heat release rate of the HTHR (as shown in Figures 1 and 2), which would reduce the maximum pressure rise rate and expand the high-load limit of HCCI.

Table 2: Combustion characteristics of PRF100 at a compression ratio of 15

| | **Case 1** | **Case 2** | **Case 3** | **Case 4** |
|---|---|---|---|---|
| **Equivalence ratio** | 0.30 | 0.33 | 0.35 | 0.37 |
| **CA 50 (deg aTDC)** | 4.7 | 5.5 | 6.0 | 5.5 |
| **IMEPn (bar)** | 2.1 | 2.6 | 2.8 | 3.0 |
| **Tint (K)** | 395 | 385 | 376 | 372 |
| **Thermal efficiency (%)** | 39.4 | 42.1 | 42.3 | 41.7 |
| **Combustion duration (CAD)** | 4.2 | 3.8 | 3.8 | 3.4 |
| **Combustion efficiency (%)** | 87.2 | 87.8 | 89.0 | 88.8 |
| **MPRR (bar/CAD)** | 2.6 | 3.2 | 3.4 | 4.3 |

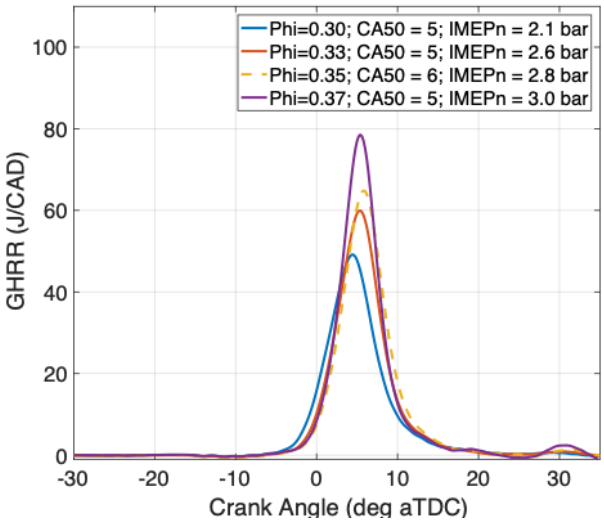


Figure 4: Gross heat release rate (GHRR) of iso-octane at a compression ratio of 15 with increasing equivalence ratio

To better understand and quantify the benefits of LTHR for expanding the high-load limit, PRF50 (50% iso-octane and 50% n-heptane) was tested at a compression ratio of 8. A similar procedure was used for PRF50 as PRF100 (iso-octane). First, the combustion phasing was kept constant at a CA50 of 5 deg aTDC to determine the highest possible load. Unlike PRF100, in PRF50, when the IMEPn of 3 bar was reached the MPRR was well below the 5 bar/CAD limit. This is due to the LTHR fraction which spreads out the heat release process and reduces the peak of the HTHR and therefore the MPRR. By adding more fuel, an IMEPn of 4.2 bar was reached, as shown in Figure 5. At a constant mass of fuel, the intake temperature was reduced to retard CA50. Unlike iso-octane, combustion was stable when CA50 was later than 6 deg aTDC due to the presence of the LTHR. Case 2 shows a CA50 of 8 degrees aTDC. Continuing the same process at a CA50 of 12.5 deg aTDC, the COV of IMEPn reached its limit of 3%. At an $IMEP_n$ of 4.3 bar and combustion efficiency of 95.1%, the latest possible CA50 for PRF50 at the compression ratio of 8 was found to be 12.5 deg aTDC, which is shown in dotted line in Figure 5. At the CA50 of 9.1 CAD, the maximum possible IMEPn was found to be 5 bar, at an intake temperature of 320 K. The other combustion characteristics of the PRF50 experiment at a compression ratio of 8 are shown in Table 3 and the GHRR is shown in Figure 5. It is important to note the maximum possible load of PRF50 at a compression ratio of 8, was limited by the intake temperature constraints. The intake temperature could not be decreased significantly further due to conduction from the engine, which resulted in the CA50 of 9.1 CAD at 5 bar IMEP. Instead of decreasing the intake temperature, the compression ratio could have been lowered. There are some experiments later in the paper with lower compression ratio; however, it is important to note that these lower compression ratios have a significant, negative impact on efficiency.

Table 3: Combustion characteristics of PRF50 at a compression ratio of 8

| | Case 1 | Case 2 | Case 3 | Case 4 |
|---|---|---|---|---|
| **Equivalence ratio** | 0.57 | 0.52 | 0.53 | 0.61 |
| **CA 50 (deg aTDC)** | 5.1 | 7.9 | 12.5 | 9.1 |
| **IMEPn (bar)** | 4.2 | 4.2 | 4.3 | 5.0 |
| **Tint (K)** | 361 | 343 | 333 | 320 |
| **Thermal efficiency (%)** | 34.4 | 36.4 | 36.1 | 35.8 |
| **Combustion duration (CAD)** | 2.4 | 3.7 | 5.7 | 2.7 |
| **Combustion efficiency (%)** | 97.3 | 95.4 | 95.1 | 97.2 |
| **Fraction of LTHR (%)** | 7.2 | 7.9 | 7.8 | 7.1 |
| **MPRR (bar/CAD)** | 6.5 | 3.38 | 1.94 | 6.1 |

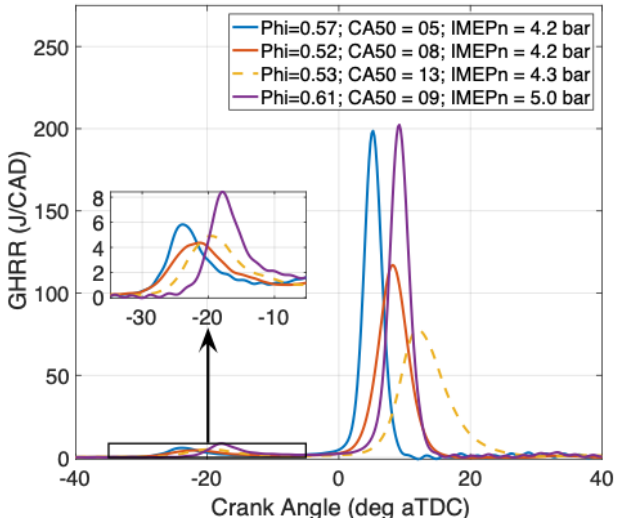


Figure 5: Gross heat release rate (GHRR) of PRF50 at a compression ratio of 8 with increasing equivalence ratio

Comparing PRF50 and PRF100 in Tables 2 and 3, at the same CA50 of 5 bar/CAD, the maximum possible IMEPn increased by 40% (from approximately 3 bar to approximately 4.2 bar). This is due to 1) the lower compression ratio (changed from 15 to 8), as it results in a larger volume at the same crank angle and results in lower pressure rise rates [51, 52], and 2) PRF50's LTHR compared to the lack of LTHR at these conditions with PRF100, which increased the LTHR fraction from approximately 0% to approximately 7%. Even though the IMEPn increases at the

constant combustion phasing, the thermal efficiency decreased by 19% (from approximately 42% to approximately 34%) due to the lower compression ratio. With PRF50, due to the LTHR produced by the pre-ignition chemistry of n-heptane, it is not only possible to achieve a higher IMEPn at a constant combustion phasing; it is also possible to achieve later combustion phasings up to a CA50 of 12.5 CAD. This in turn helps expand the maximum possible IMEPn further, up to 5 bar. Other researchers have also noted and studied the ability of combustion phasing to extend the high load limit of HCCI [2]. The energy released during the LTHR provided enough energy to start the HTHR at later combustion phasings, which was a major contributing factor in expanding the high-load limit of HCCI. This is due to the temperature and pressure increase from the LTHR which helps to trigger the HTHR. Contrarily, in PRF100, the rise in temperature to reach autoignition will be achieved exclusively by the compression process. Thus, combustion cannot start significantly after TDC.

Following the PRF50 experiments, PRF0 (n-heptane) was studied at a compression ratio of 6.5 to find the maximum possible load and the latest possible CA50. The results are tabulated in Table 4 and the GHRRs are shown in Figure 6. PRF0 (pure n-heptane) was expected to have the highest percentage of LTHR. Therefore, it is expected to enable later CA50 phasings, which can further increase the maximum possible load.

Similar to the previous experiments, a constant CA50 combustion phasing of 5 deg aTDC was maintained and the maximum possible load was determined. Cases 1 and 3 in Table 4 show two different load levels at a CA50 of around 5 deg aTDC. Unlike the higher PRF numbers, the MPRR was below 5 bar/CA with a CA50 of 5 deg aTDC. The main reason was the lower compression ratio, as discussed previously, and the higher fraction of LTHR of PRF0. As the fraction of LTHR increases, the fraction of HTHR decreases, which reduces the peak pressure rise rate. Although the MPRR limit was not achieved, the intake temperature could not be decreased further below 313 K. Therefore, both PRF50 and PRF0 were limited by the intake temperature rather than the MPRR limit and stability limit. Due to this experimental limitation, it was not possible to reach the MPRR limit without advancing the combustion phasing. This results in the maximum possible IMEPn of PRF0 at a compression ratio of 6.5 to be 4.4 bar (Case 3 in Table 4).

Since the maximum load was limited by the intake temperature, the latest possible CA50 was found by decreasing the mass of fuel slightly to delay combustion phasing. As the mass of fuel decreased by 5% with a constant intake temperature, the CA50 retarded by 11 CAD, which is shown as Case 2 in Table 4. This CA50 timing is significantly later than PRF100, and still considerably later than PRF50. Similar to PRF50, for Case 2, the HTHR starts after TDC, due to the LTHR produced by the pre-ignition kinetics of n-heptane. Even with a CA50 of 16, the combustion efficiency did not suffer (95.7%). It is also interesting to note that in this case, at a constant intake temperature, the start of LTHR changed (unlike Figure 2 where the LTHR stayed constant with constant intake temperature). This result shows that the start of LTHR depends on both the intake temperature and the equivalence ratio.

Table 4: Combustion characteristics of PRF 0 at a compression ratio of 6.5

| | **Case 1** | **Case 2** | **Case 3** |
|---|---|---|---|
| **Equivalence ratio** | 0.51 | 0.51 | 0.54 |
| **CA 50 (deg aTDC)** | 5.5 | 16.0 | 4.7 |
| **IMEPn (bar)** | 4.0 | 4.3 | 4.4 |
| **Tint (K)** | 331 | 313 | 313 |
| **Thermal efficiency (%)** | 35.7 | 36.2 | 34.9 |
| **Combustion duration (CAD)** | 3.7 | 2.7 | 5.7 |
| **Combustion efficiency (%)** | 96.1 | 95.7 | 96.4 |
| **Fraction of LTHR (%)** | 10.2 | 11.0 | 10.3 |
| **MPRR (bar/CAD)** | 2.88 | 1.19 | 3.42 |

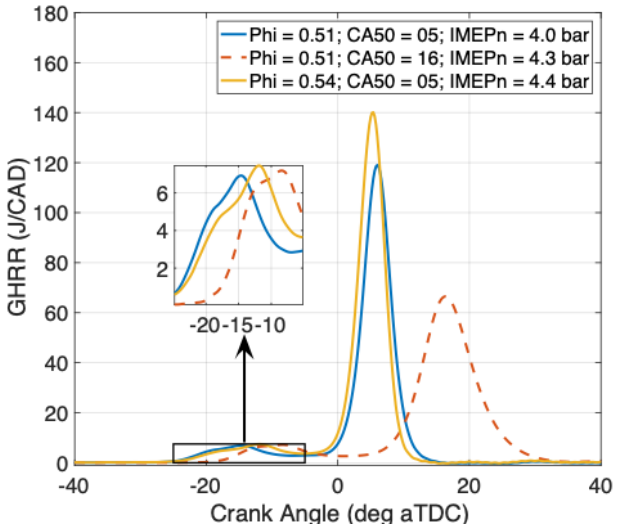


Figure 6: Gross heat release rate (GHRR) of PRF0 at a compression ratio of 6.5 with the latest possible CA 50

Although the latest possible CA50 for PRF0 was later than that of PRF50, the maximum possible load was less due to the experimental limitation on the intake temperature. Since the intake temperature could not be decreased further, an alternative approach would be to decrease the compression ratio further (below 6.5). However, decreasing the compression ratio will also decrease the expansion ratio, thereby reducing the thermal efficiency. As evidence of this effect, the thermal efficiencies from Table 2 with a compression ratio of 15 were approximately 42%. As the compression ratio decreased from 15 to 8 (and the PRF number decreased from 100 to 50), the thermal efficiency

decreased to approximately 36% (Table 3). Finally, decreasing the compression ratio to 6.5 further lowered the thermal efficiency to 35% (shown in Table 5 below).

Beyond the fact that the efficiency decreases with compression ratio, the fraction of LTHR is also affected by the cylinder pressure at the time of ignition. Therefore, the compression ratio plays a role in the fraction of the total heat release that is LTHR. From Table 4, it can be seen that the fraction of LTHR was less than 11%, which was lower than expected for PRF0 based on the previous results shown in Figure 1 where PRF13 exhibited a 12.8% fraction of LTHR at the compression ratio of 9. Since the motivation of this work is to expand the high load limit of HCCI by reducing the peak of the HTHR and increasing the peak of LTHR, it is important to understand these differences in the LTHR fraction. To understand how the difference in the pressure at the start of combustion affects the fraction of LTHR of PRF0, PRF0 fuel blend was tested at four different compression ratios.

The combustion characteristics of PRF0 were tested with four different compression ratios from 6.5 to 8 in increments of 0.5 to determine the trends of the heat release characteristics. Since the compression ratios are different, the heat release will be affected by the temperature and the pressure at the start of combustion. The temperature at the start of combustion was kept constant for varying compression ratio to study the effect of pressure at the start of combustion on the LTHR fraction. Table 5 shows the combustion characteristics of PRF0 at four different compression ratios with varying intake temperatures and equivalence ratios. Since this comparison is designed to understand the effects of compression ratio on the LTHR fraction, the four chosen cases are not at the peak operating load. Instead, they were chosen at the equivalence ratios and intake temperatures where the temperature at SOC are same. Since, the temperature at the SOC is maintained constant at varying compression ratio, the equivalence ratios are different to maintain constant combustion phasing with the CA50 of 5 deg aTDC.

By comparing the four cases in Table 5 and Figure 7, it can be seen that the highest compression ratio of 8 has the highest LTHR fraction of approximately 12%. Along with the LTHR fraction, the highest compression ratio also has the highest thermal efficiency, due to the higher expansion ratio. In order to understand the LTHR, the gross heat release rates of the varying compression ratio cases are plotted in Figure 7. Although the equivalence ratio and compression ratio were changing, the peak of the LTHR rate was constant, whereas the peak of the HTHR rate increased from 45 J/CAD to 110 J/CAD. The increase in HTHR is due to the increase in mass of fuel. However, from these results, only the peak of the HTHR is affected, while the peak of the LTHR is constant. If the peak of the LTHR had also increased, the peak of the HTHR would not have increased as significantly. This result will be explored in more detail in the following section, but it is important to note that this effect limits the efficacy of the approach described in this paper (i.e., using the LTHR to extend the latest possible CA50 and extend the high load limit).

Table 5: Combustion characteristics of PRF0 at varying compression ratio

| | Case 1 | Case 2 | Case 3 | Case 4 |
|---|---|---|---|---|
| **Compression ratio** | 6.5 | 7 | 7.5 | 8 |
| **Equivalence ratio** | 0.49 | 0.44 | 0.37 | 0.34 |
| **CA 50 (deg aTDC)** | 5.2 | 4.8 | 4.4 | 4.5 |
| **IMEPn (bar)** | 3.8 | 3.5 | 3.0 | 2.7 |
| **Tint (K)** | 347 | 348 | 348 | 345 |
| **Thermal efficiency (%)** | 35.1 | 37.0 | 38.7 | 38.8 |
| **Combustion duration (CAD)** | 3.9 | 4.1 | 4.7 | 5.9 |
| **Combustion efficiency (%)** | 96.2 | 95.8 | 93.9 | 91.6 |
| **Fraction of LTHR (%)** | 10.5 | 9.8 | 11.3 | 12.1 |
| **MPRR (bar/CAD)** | 2.62 | 2.36 | 1.94 | 1.42 |

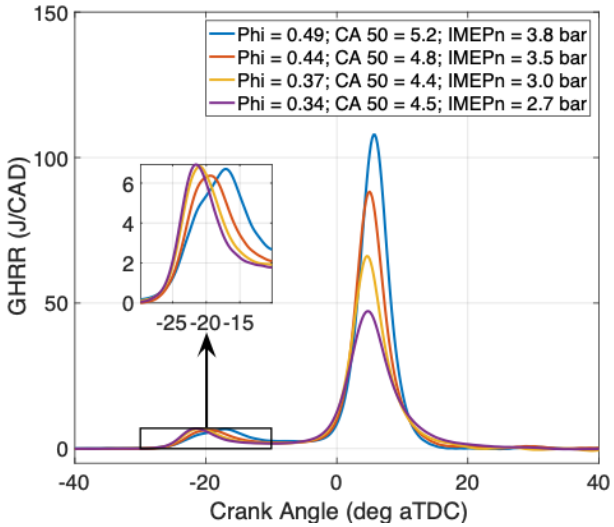


Figure 7: Gross heat release rate (GHRR) of PRF 0 at a constant temperature at the start of combustion, but varying compression ratio and equivalence ratio

Since the results in Figure 7 are critical for understanding the ability of LTHR to extend the range of possible combustion phasings and loads, but the interdependencies of intake temperature, equivalence ratio, and compression ratio on the heat release characteristics are difficult to isolate using experiments alone, a single-zone chemical kinetics model was used to understand the effects of the compression ratio and equivalence ratio on the heat release characteristics and LTHR fraction.

Using a MATLAB-based, chemical kinetics simulation code coupled to Cantera, the heat release characteristics were calculated. Since it is a single-zone simulation, each case was initialized with the pressure and temperature at the start of combustion calculated from the experimental results. The effects of different compression ratios were simulated by varying the pressure at the start of the simulation based on the pressure at the start of combustion for the different compression ratio cases. The simulated heat release rates were normalized by the energy input to remove the effect of the amount of trapped fuel on the peak of the heat release rate. Figure 8 shows the normalized heat release rates of PRF0 at constant temperature and pressure at the start of combustion, while varying the equivalence ratio; Figure 9 shows the normalized heat release rates of PRF0 at constant temperature at the start of combustion and equivalence ratio, while varying the pressure at the start of combustion.

From examining the results of the single-zone chemical kinetics model in Figures 8 and 9, it becomes clear that the pressure at start of combustion and the equivalence ratio have different effects on the start of LTHR and HTHR, and the fraction of LTHR in the overall heat released. Increasing the equivalence ratio by 67% from 0.3 to 0.5, at a constant initial pressure and temperature, results in:

- An advance of the LTHR by 4%,
- An advance of the HTHR by 57%,
- A decrease in the fraction of LTHR by 52%.

Similarly, increasing the pressure at the start of combustion by 50%, which corresponds to the compression ratio change from 6.5 to 8, results in:

- An advance of the LTHR by 3%,
- An advance of the HTHR by 32%,
- A decrease in the fraction of LTHR by 16%

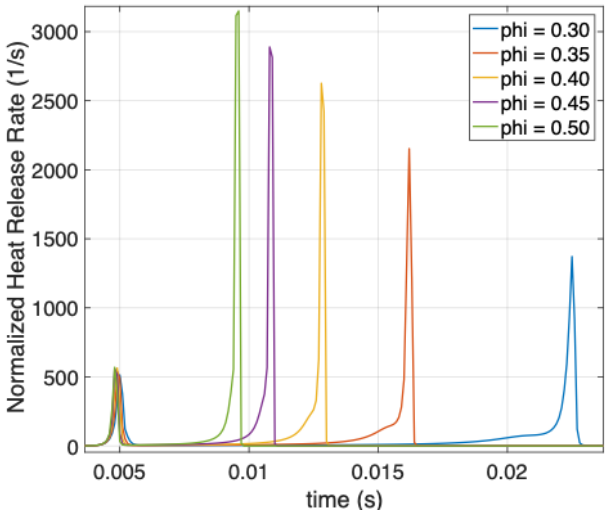


Figure 8: Normalized Heat Release Rate at constant pressure at the start of combustion of 8 bar, and temperature at the start of combustion of 690 K

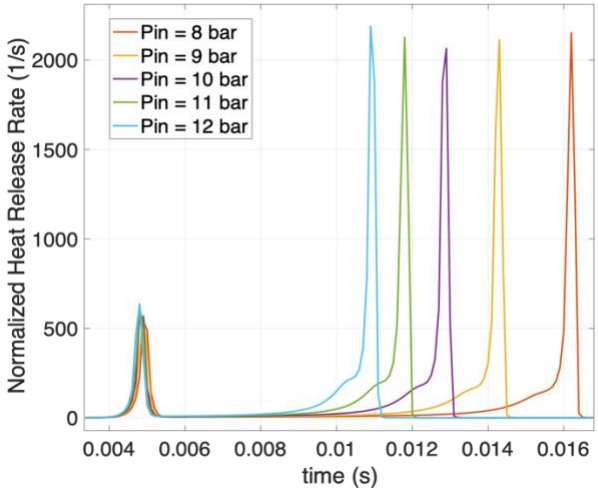


Figure 9: Normalized Heat Release Rate at a constant equivalence ratio of 0.35 and temperature at the start of combustion of 690 K

Similar trends were previously observed and reported by other researchers when studying the LTHR dependency, ignition delay, and the start of LTHR and HTHR over various equivalence ratios, pressures, intake temperatures, and engine speeds [53 – 55]. Considering the heat release rates of PRF0 at varying compression ratio in Figure 7, as the compression ratio increases (and the pressure at SOC increases), the equivalence ratio decreases. Since the maximum possible load was limited by the maximum pressure rise rate at higher compression ratios, the compression ratio was decreased. However, this resulted in a lower fraction of LTHR, as shown in Table 5. Since the main goal of this approach is to take advantage of the fraction of LTHR to achieve higher loads, lowering the compression ratio and its effect

on the fraction of LTHR restricts the maximum possible load and mitigates the efficacy of this approach.

To understand the trends of LTHR fraction more clearly, the single-zone chemical kinetics model was used to simulate a large number of equivalence ratios and initial pressures, at constant initial temperatures of 690 K. The results are presented in the form of a contour plots in Figure 10. Additionally, the cases in Table 5 are superimposed on the contour map as the red squares in Figure 10 based on their equivalence ratio and pressure at the start of LTHR.

From the contour plot, it can be seen that the LTHR fraction depends highly on the equivalence ratio and somewhat on the pressure at the start of combustion. Using this contour plot, the heat release rates of the four PRF0 cases at different compression ratios and equivalence ratios can be understood better. It can be seen from the plot that lowering the compression ratio and therefore lowering the pressure at the start of LTHR results in a lower fraction of LTHR. Additionally, increasing the equivalence ratio results in a significantly lower fraction of LTHR. Also, the interdependency of equivalence ratio and compression ratio (pressure at start of combustion) can be removed from this contour plot. If the equivalence ratio was kept constant at 0.35 and the compression ratio was changed from 8 to 6.5, the pressure at the start of combustion would have decreased by 17%, which causes the LTHR fraction to decrease by 2% (from approximately 18.4% to approximately 18%). On the other hand, if the compression ratio was kept constant at 8 and the equivalence ratio changes from 0.35 to 0.5, the LTHR fraction decreases by 15%. Therefore, even though lowering the compression ratio extends the maximum possible load before reaching the MPRR limit, the lower pressure at the start of combustion and higher equivalence ratio reduce the fraction of LTHR significantly and limit the maximum possible IMEPn.

Finally, from Figure 10, it can be observed that the trend of the LTHR fraction as predicted by the single-zone chemical kinetics model generally agrees with the experimental results. The magnitude of the LTHR fractions are different, due to the single-zone simulation's uniform temperature which does not accurately replicate the experimental conditions. However, the fact that the trend is well captured by the chemical kinetics indicates that the cause of the experimentally observed trend is the chemical kinetics and the impact of pressure and equivalence ratio on the chemical kinetics.

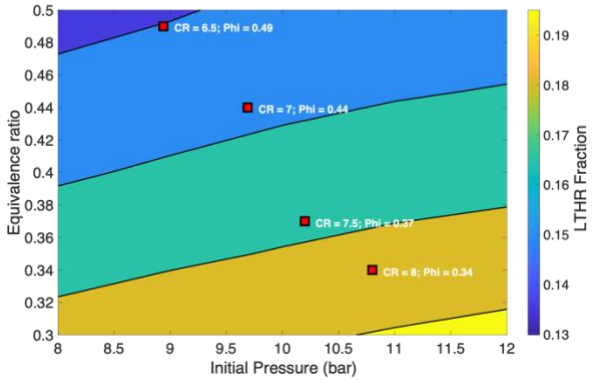

Figure 10: Trend LTHR fraction for varying pressure at start of combustion and equivalence ratio

## Conclusion:

At a constant equivalence ratio and compression ratio, increasing the amount of n-heptane (decreasing the PRF number) increases the fraction of LTHR, increases the peak of LTHR, and decreases the peak of HTHR. This showed that by increasing the fraction of LTHR, the peak of HTHR is lower and the high load-limit can be extended by elongating the energy release process. Also, the LTHR can allow the HTHR to start significantly after TDC and retard the combustion phasing later than what would be possible with a single-stage ignition fuel. To analyze these effects in more detail, three different PRF blends were studied in HCCI combustion on a single cylinder, variable compression ratio CFR engine. Additionally, a single-zone chemical kinetic model was used to help complement the experiments. The following conclusions can be drawn from the results:

1. With a single-stage ignition fuel and a relatively high compression ratio, the maximum possible load was relatively low before the pressure rise rate limit was reached. Additionally, the latest possible combustion phasing was limited by variability. The start of heat release needed to occur before TDC.
2. The use of two-stage ignition fuels with lower compression ratios significantly extends the high-load limit because a fraction of energy was released as LTHR, which reduces the peak of the HTHR. With the help of the LTHR fraction, the latest possible combustion phasing was extended significantly later before being limited by the COV of IMEP. The later combustion phasings themselves allow the high-load limit to be extended further. However, the thermal efficiency decreased due to the decreasing compression ratio.
3. For lower PRF number blends, the maximum possible operating load is limited by practical constraints on the intake temperature.
4. The goal of this approach is to use the two-stage ignition characteristics of certain fuels to enable later combustion phasings and extend the high-load limit. The approach was determined to be effective. However, as the compression ratio was lowered to allow for lower

PRF number blends and the equivalence ratio increased, the fraction of LTHR decreased, which mitigated the efficacy of this approach. This effect was determined to be attributed to the chemical kinetics, since a single-zone chemical kinetics simulation was able to capture the trends of the experiment.

## References:


1. Dec, J. E., Hwang, W., & Sjöberg, M. (2006). An investigation of thermal stratification in HCCI engines using chemiluminescence imaging (No. 2006-01-1518). SAE Technical Paper
2. Sjöberg, M., Dec, J. E., & Cernansky, N. P. (2005). Potential of thermal stratification and combustion retard for reducing pressure-rise rates in HCCI engines, based on multi-zone modeling and experiments (No. 2005-01-0113). SAE Technical Paper
3. Flowers, D. L., Aceves, S. M., Martinez-Frias, J., & Dibble, R. W. (2002). Prediction of carbon monoxide and hydrocarbon emissions in iso-octane HCCI engine combustion using multizone simulations. Proceedings of the Combustion Institute, 29(1), 687-694.
4. Jun, D., Ishii, K., & Iida, N. (2003). Combustion analysis of natural gas in a four stroke HCCI engine using experiment and elementary reactions calculation (No. 2003-01-1089). SAE Technical Paper
5. Battin-Leclerc, F. (2008). Detailed chemical kinetic models for the low-temperature combustion of hydrocarbons with application to gasoline and diesel fuel surrogates. Progress in Energy and Combustion Science, 34(4), 440-498
6. Zádor, J., Taatjes, C. A., & Fernandes, R. X. (2011). Kinetics of elementary reactions in low-temperature autoignition chemistry. Progress in Energy and Combustion Science, 37(4), 371-421
7. Lawler, B., Hoffman, M., Filipi, Z., Güralp, O., & Najt, P. (2012). Development of a postprocessing methodology for studying thermal stratification in an HCCI engine. Journal of Engineering for Gas Turbines and Power, 134(10), 102801
8. Lawler, B., Lacey, J., Güralp, O., Najt, P., & Filipi, Z. (2018). HCCI combustion with an actively controlled glow plug: The effects on heat release, thermal stratification, efficiency, and emissions. Applied Energy, 211, 809-819
9. Komninos, N. P. (2015). The effect of thermal stratification on HCCI combustion: a numerical investigation. Applied Energy, 139, 291-302
10. Dec, J. E., & Hwang, W. (2009). Characterizing the development of thermal stratification in an HCCI engine using planar-imaging thermometry. SAE International Journal of Engines, 2(1), 421-438
11. Dronniou, N., & Dec, J. (2012). Investigating the development of thermal stratification from the near-wall regions to the bulk-gas in an HCCI engine with planar imaging thermometry. SAE International Journal of Engines, 5(3), 1046-1074.
12. Sjöberg, M., & Dec, J. E. (2005). Effects of engine speed, fueling rate, and combustion phasing on the thermal stratification required to limit HCCI knocking intensity (No. 2005-01-2125). SAE Technical Paper
13. Dec, J. E. (2009). Advanced compression-ignition engines—understanding the in-cylinder processes. Proceedings of the combustion institute, 32(2), 2727-2742.
14. Saxena, S., & Bedoya, I. D. (2013). Fundamental phenomena affecting low temperature combustion and HCCI engines, high load limits, and strategies for extending these limits. Progress in Energy and Combustion Science, 39(5), 457-488.
15. Dec, J. E., Hwang, W., & Sjöberg, M. (2006). An investigation of thermal stratification in HCCI engines using chemiluminescence imaging (No. 2006-01-1518). SAE Technical Paper.
16. Sjöberg, M., Dec, J. E., Babajimopoulos, A., & Assanis, D. N. (2004). Comparing enhanced natural thermal stratification against retarded combustion phasing for smoothing of HCCI heat-release rates (No. 2004-01-2994). SAE Technical Paper.
17. Dec, J. E., & Hwang, W. (2009). Characterizing the development of thermal stratification in an HCCI engine using planar-imaging thermometry. SAE International Journal of Engines, 2(1), 421-438.
18. Sjöberg, M., Dec, J. E., & Cernansky, N. P. (2005). Potential of thermal stratification and combustion retard for reducing pressure-rise rates in HCCI engines, based on multi-zone modeling and experiments (No. 2005-01-0113). SAE Technical Paper.
19. Lawler, B., Splitter, D., Szybist, J., & Kaul, B. (2017). Thermally Stratified Compression Ignition: A new advanced low temperature combustion mode with load flexibility. Applied energy, 189, 122-132.
20. Rahimi Boldaji, M., Sofianopoulos, A., Mamalis, S., & Lawler, B. (2018). Computational fluid dynamics investigations of the effect of water injection timing on thermal stratification and heat release in thermally stratified compression ignition combustion. International Journal of Engine Research, 1468087418767451.
21. Boldaji, M. R., Sofianopoulos, A., Mamalis, S., & Lawler, B. (2018). Effects of Mass, Pressure, and Timing of Injection on the Efficiency and Emissions Characteristics of TSCI Combustion with Direct Water Injection (No. 2018-01-0178). SAE Technical Paper.
22. Gainey, B., Hariharan, D., Yan, Z., Zilg, S., Rahimi Boldaji, M., & Lawler, B. (2018). A split injection of wet ethanol to enable thermally stratified compression ignition. International Journal of Engine Research, 1468087418810587.
23. Boldaji, M. R., Gainey, B., & Lawler, B. (2019). Thermally stratified compression ignition enabled by wet ethanol with a split injection strategy: A CFD simulation study. Applied Energy, 235, 813-826.
24. Sjöberg, M., & Dec, J. E. (2003). Combined effects of fuel-type and engine speed on intake temperature requirements and completeness of bulk-gas reactions for HCCI combustion (No. 2003-01-3173). SAE Technical Paper
25. Sjoberg, M., & Dec, J. E. (2010). Ethanol autoignition characteristics and HCCI performance for wide ranges of engine speed, load, and boost. SAE International Journal of Engines, 3(1), 84-106

26. Dec, J. E., & Yang, Y. (2010). Boosted HCCI for high power without engine knock and with ultra-low NOx emissions-using conventional gasoline. SAE International Journal of Engines, 3(1), 750-767
27. Dec, J. E., Yang, Y., & Dronniou, N. (2012). Improving efficiency and using E10 for higher loads in boosted HCCI engines. SAE International Journal of Engines, 5(3), 1009-1032
28. Wolk, B., & Chen, J. Y. (2014). Computational study of partial fuel stratification for HCCI engines using gasoline surrogate reduced mechanism. Combustion Science and Technology, 186(3), 332-354.
29. Inagaki, K., Fuyuto, T., Nishikawa, K., Nakakita, K., & Sakata, I. (2006). Dual-fuel PCI combustion controlled by in-cylinder stratification of ignitability (No. 2006-01-0028). SAE Technical Paper
30. Wada, Y., & Senda, J. (2009). Demonstrating the potential of mixture distribution control for controlled combustion and emissions reduction in premixed charge compression ignition engines (No. 2009-01-0498). SAE Technical Paper
31. Dahl, D., Andersson, M., Berntsson, A., Denbratt, I., & Koopmans, L. (2009). Reducing pressure fluctuations at high loads by means of charge stratification in HCCI combustion with negative valve overlap (No. 2009-01-1785). SAE Technical Paper
32. Yang, Y., Dec, J., Dronniou, N., & Cannella, W. (2012). Boosted HCCI combustion using low-octane gasoline with fully premixed and partially stratified charges. SAE International Journal of Engines, 5(3), 1075-1088
33. Dec, J. E., & Sjöberg, M. (2004). Isolating the effects of fuel chemistry on combustion phasing in an HCCI engine and the potential of fuel stratification for ignition control (No. 2004-01-0557). SAE Technical Paper
34. Dec, J. E., Yang, Y., & Dronniou, N. (2011). Boosted HCCI-controlling pressure-rise rates for performance improvements using partial fuel stratification with conventional gasoline. SAE International Journal of Engines, 4(1), 1169-1189
35. Yang, Y., Dec, J. E., Dronniou, N., & Sjöberg, M. (2011). Tailoring HCCI heat-release rates with partial fuel stratification: Comparison of two-stage and single-stage-ignition fuels. Proceedings of the Combustion Institute, 33(2), 3047-3055
36. Sjöberg, M., & Dec, J. E. (2006). Smoothing HCCI heat-release rates using partial fuel stratification with two-stage ignition fuels (No. 2006-01-0629). SAE Technical Paper
37. Tanaka, S., Ayala, F., Keck, J. C., & Heywood, J. B. (2003). Two-stage ignition in HCCI combustion and HCCI control by fuels and additives. Combustion and flame, 132(1-2), 219-23
38. Cox, R. A., & Cole, J. A. (1985). Chemical aspects of the autoignition of hydrocarbon-air mixtures. Combustion and Flame, 60(2), 109-123
39. Hessel, R. P., Foster, D. E., Aceves, S. M., Davisson, M. L., Espinosa-Loza, F., Flowers, D. L., … & Babajimopoulos, A. (2008). Modeling iso-octane HCCI using CFD with multi-zone detailed chemistry; comparison to detailed speciation data over a range of lean equivalence ratios (No. 2008-01-0047). SAE Technical Paper.
40. Yang, R., Hariharan, D., Zilg, S., Lawler, B., & Mamalis, S. (2018). Efficiency and Emissions Characteristics of an HCCI Engine Fueled by Primary Reference Fuels.
41. Zheng, J., Yang, W., Miller, D. L., & Cernansky, N. P. (2001). Prediction of pre-ignition reactivity and ignition delay for HCCI using a reduced chemical kinetic model (No. 2001-01-1025). SAE Technical Paper.
42. Epping, K., Aceves, S., Bechtold, R., & Dec, J. E. (2002). The potential of HCCI combustion for high efficiency and low emissions (No. 2002-01-1923). SAE Technical Paper.
43. Tanaka, S., Ayala, F., & Keck, J. C. (2003). A reduced chemical kinetic model for HCCI combustion of primary reference fuels in a rapid compression machine. Combustion and flame, 133(4), 467-481.
44. Shibata, G., Oyama, K., Urushihara, T., & Nakano, T. (2004). The effect of fuel properties on low and high temperature heat release and resulting performance of an HCCI engine (No. 2004-01-0553). SAE Technical Paper.
45. Vuilleumier, D., Atef, N., Kukkadapu, G., Wolk, B., Selim, H., Kozarac, D., … & Sarathy, S. M. (2018). The Influence of Intake Pressure and Ethanol Addition to Gasoline on Single-and Dual-Stage Autoignition in an HCCI Engine. Energy & Fuels, 32(9), 9822-9837.
46. Sjöberg, M., & Dec, J. E. (2007). Comparing late-cycle autoignition stability for single-and two-stage ignition fuels in HCCI engines. Proceedings of the combustion institute, 31(2), 2895-2902.
47. Brettschneider, J. (1997). Extension of the equation for calculation of the air-fuel equivalence ratio (No. 972989). SAE Technical Paper.
48. Chang, J., Güralp, O., Filipi, Z., Assanis, D. N., Kuo, T. W., Najt, P., & Rask, R. (2004). New heat transfer correlation for an HCCI engine derived from measurements of instantaneous surface heat flux (No. 2004-01-2996). SAE Technical paper.
49. Goodwin, D. G., Moffat, H. K., & Speth, R. L. (2009). Cantera: An object-oriented software toolkit for chemical kinetics, thermodynamics, and transport processes. Caltech, Pasadena, CA.
50. Wang, H., Yao, M., & Reitz, R. D. (2013). Development of a reduced primary reference fuel mechanism for internal combustion engine combustion simulations. Energy & Fuels, 27(12), 7843-7853.
51. Lawler, B., Joshi, S., Lacey, J., Guralp, O., Najt, P., & Filipi, Z. (2014, October). Understanding the effect of wall conditions and engine geometry on thermal stratification and HCCI combustion. In ASME 2014 Internal Combustion Engine Division Fall Technical Conference (pp. V001T03A020-V001T03A020). American Society of Mechanical Engineers.
52. Olsson, J. O., Tunestål, P., Johansson, B., Fiveland, S., Agama, R., Willi, M., & Assanis, D. N. (2002). Compression ratio influence on maximum load of a natural gas fueled HCCI engine (No. 2002-01-0111). SAE Technical Paper.
53. Kumar, K., Mittal, G., & Sung, C. J. (2009). Autoignition of n-decane under elevated pressure and low-to-intermediate temperature conditions. Combustion and Flame, 156(6), 1278-1288.

54. Kumar, K., & Sung, C. J. (2010). An experimental study of the autoignition characteristics of conventional jet fuel/oxidizer mixtures: Jet-A and JP-8. Combustion and Flame, 157(4), 676-685.
55. Weber, B. W., Kumar, K., Zhang, Y., & Sung, C. J. (2011). Autoignition of n-butanol at elevated pressure and low-to-intermediate temperature. Combustion and flame, 158(5), 809-819.

## Contact Information:

Deivanayagam Hariharan:
deivanayagam.hariharan@stonybrook.edu,
deivanayagam.hariharan@gmail.com

Benjamin Lawler: benjamin.lawler@stonybrook.edu

## Acknowledgments:

The author would like to thank Brian Gainey, Graduate Student at Stony Brook University for constructive criticism of the manuscript.

## Abbreviations:

| | |
|---|---|
| **HCCI** | Homogeneous Charge Compression Ignition |
| **LTC** | Low Temperature Combustion |
| **SOC** | Start of Combustion |
| **MEP** | Mean Effective Pressure |
| **IMEPn** | Net Indicated Mean Effective Pressure |
| **THC** | Total unburned Hydrocarbons |
| **MPRR** | Maximum Pressure Rise Rate |
| **PFS** | Partial Fuel Stratification |
| **TDC** | Top Dead Center |
| **PRF** | Primary Reference Fuels |
| **LTHR** | Low Temperature Heat Release |
| **HTHR** | High Temperature Heat Release |
| **CFR** | Cooperative Fuel Research |
| **GHRR** | Gross Heat Release Rate |
| **deg aTDC** | Degrees after Top Dead Center |
| **CAD** | Crank Angle Degrees |
| **PRFx** | x is the percentage of Iso-octane in the mixture of Iso-octane and n-heptane |
| **COV** | Coefficient of Variance |
| **Pin** | Initial Pressure |